

# Application of Novel Constrained Groove Pressing Routes on Austenitic Stainless Steel

Zeynel Guler<sup>1</sup> · Guney Guven Yapici<sup>1,2</sup> 

Received: 9 February 2021 / Accepted: 9 June 2021 / Published online: 6 July 2021  
© The Indian Institute of Metals - IIM 2021

**Abstract** In this study, a novel set of constrained groove processing routes was put forward especially to underline the variation of strain paths. Namely, 304 stainless steel sheets were processed by five distinctly specified constrained groove pressing routes. The enhancement of mechanical properties along with anisotropic behavior after each pass were compared for each route. Significant elevation in the hardness and tensile strength was observed after the initial pass while the successive passes demonstrated relatively less increase. Notable improvements in tensile strengths were observed for route E and C along two perpendicular directions up to 30% and 40%, respectively. Route A displayed the highest anisotropy in relation with its processing scheme. Microstructural evolution during processing was examined indicating slight refinement irrespective of the strain path.

**Keywords** Steel · Constrained groove pressing · Severe plastic deformation · Anisotropy · Strength · Strain path

## 1 Introduction

Stainless steel 304 is one of the most commonly used engineering materials in the manufacturing industry. It constitutes roughly 50% of stainless steel production and finds place in a variety of applications, especially in sheet form. Therefore, improving the mechanical properties would be beneficial in terms of cost-effective and light designs. In the present work, constrained groove pressing, introduced by Shin et al. as a severe plastic deformation (SPD) technique, is applied to modify the mechanical behavior [1].

SPD is a top-down approach for the fabrication of materials with ultrafine and/or nanoscale microstructures [2]. Various SPD methods have been developed, examined and evaluated over the last decade ranging from friction stir processing (FSP) [3, 4], equal channel angular extrusion (ECAE/P) [5, 6] and high pressure torsion (HPT) [7, 8] for bulk deformation to accumulative roll bonding (ARB) [9, 10] and constrained groove pressing (CGP) [11] for sheet metal forming. Among the sheet metal processing methods, CGP is one of the mostly utilized for reaching superior properties. It provides a significant amount of strain while preventing substantial change in sample dimensions.

The effects of CGP process on various materials, such as steel [12], copper [13, 14], magnesium alloys [15] and aluminum alloys [16], have been investigated from different perspectives. Typically, single to several CGP passes have been applied at various temperatures depending on the material in study. Hardness got improved about one and a half times with an acceptable uniformity, accompanied by about three times strength increase for commercially pure aluminum after an effective strain of 4.64 [1]. Similarly, CGP provided low carbon steel with 100% increase

---

✉ Guney Guven Yapici  
guven.yapici@ozyegin.edu.tr

<sup>1</sup> Mechanical Engineering Department, Ozyegin University, Istanbul, Turkey

<sup>2</sup> Mechanics and Manufacturing of Functional and Structural Materials Laboratory (MEMFIS), Ozyegin University, Istanbul, Turkey

in yield strength and hardness values. In addition, non-uniformity of the mechanical properties decreased with the implementation of cross-route pressing [12]. In another work on low carbon steel, the effect of post-CGP annealing was investigated. It was disclosed that annealing effectively helped to recover the ductility of the severely deformed material [17]. For commercially pure copper subjected to a strain level of 3.48, hardness and yield strength were improved nearly two-folds and three-folds, respectively [13]. 30% increase in the microhardness was detected for the twin-roll cast AZ31 magnesium alloy after one cycle of CGP [15]. Recently, strength improvement over 1 GPa was obtained for AISI 304 after two CGP passes with a significant loss of ductility [18].

Although CGP has been a topic of interest in a number of materials, there has been a lack of research into the deformation characteristics of austenitic stainless steels and more specifically on the resulting anisotropy. Novelty of this work stems from the successful implementation of a unique and systematic set of processing routes to four passes. The influence of these routes on microstructural evolution and mechanical properties is underlined in a comparative manner for an austenitic stainless steel, which is rarely investigated in this scope, albeit its wide utilization in various industrial settings.

## 2 Experimental Procedure

The deformation principle and relevant geometrical parameters of a CGP die are shown in Fig. 1a. The groove width ( $w$ ), distance between grooves ( $d$ ) and groove height ( $h$ ) are designed as 2 mm in this study. During pressing, corrugation takes place which is followed by straightening to flatten the surface of the sample as indicated by steps 1 and 2 in Fig. 1a. This imparts a reverse shear deformation

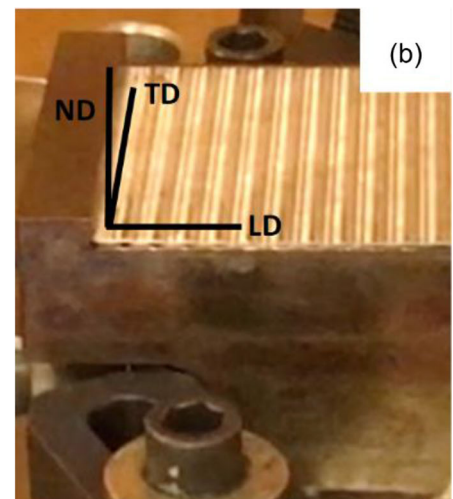
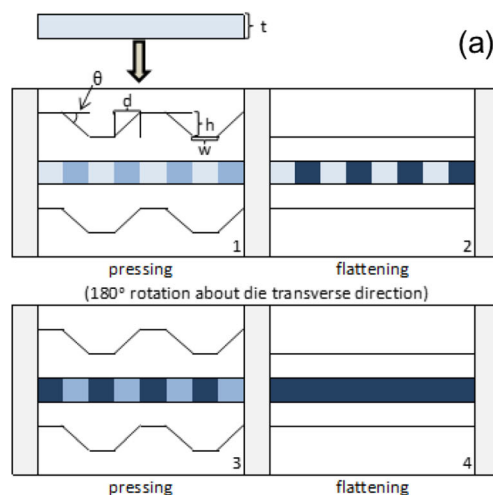
on the already deformed area while the undeformed area remains unaffected. Uniform straining is possible by rotating the sample by  $180^\circ$  about the transverse direction after each corrugation and flattening. The identical corrugation and flattening operations are implemented for the undeformed region as indicated by steps 3 and 4 in Fig. 1a. This sequence of 4 pressing operations as a whole constitutes a single CGP pass.

AISI 304 stainless steel sheets with the chemical composition in mass% as 18.19 Cr, 8.14 Ni, 1.53 Mn, 0.018 C and Fe balance were received in annealed condition and processed at ambient temperature and at a rate of 1 mm/s. Sheet surfaces were coated with a thin layer of lubricant to reduce the detrimental effects of friction between the die and the specimen leading to micro-cracks on the surface of sheets resulting in a relatively high residual stress particularly for further passes [19]. Five square plates with 1 mm thickness and surface area of  $0.01\text{m}^2$  were prepared to analyze the effects of different routes as specified in Fig. 2. Difference among the routes proceeded from the alternative rotations of the samples about the normal direction. The routes have been introduced for enabling abrupt strain path changes after each pass.

The motivation of this approach is to demonstrate the effect of processing path on the mechanical properties with regard to directionality. In route A, groove edges were consistently in line with the transverse direction (TD) of the sheet during pressings. Routes B-E imposed in-plane rotations of the sheet between CGP passes. Two parallel and two perpendicular passes with respect to groove edges were applied for routes B and D in different orders. On the other hand, routes C and E enabled to analyze the effect of pass quantity for specific pressing directions.

Vickers microhardness measurements were recorded under 1 kgf load with a holding time of 10 s. Values were obtained at 10 mm intervals along the longitudinal

**Fig. 1** a Schematic representation of the geometrical parameters of the die and a single pass of a CGP Route, b CGP die with specific material directions, where ND is the normal direction, LD is the longitudinal direction and TD is the transverse direction



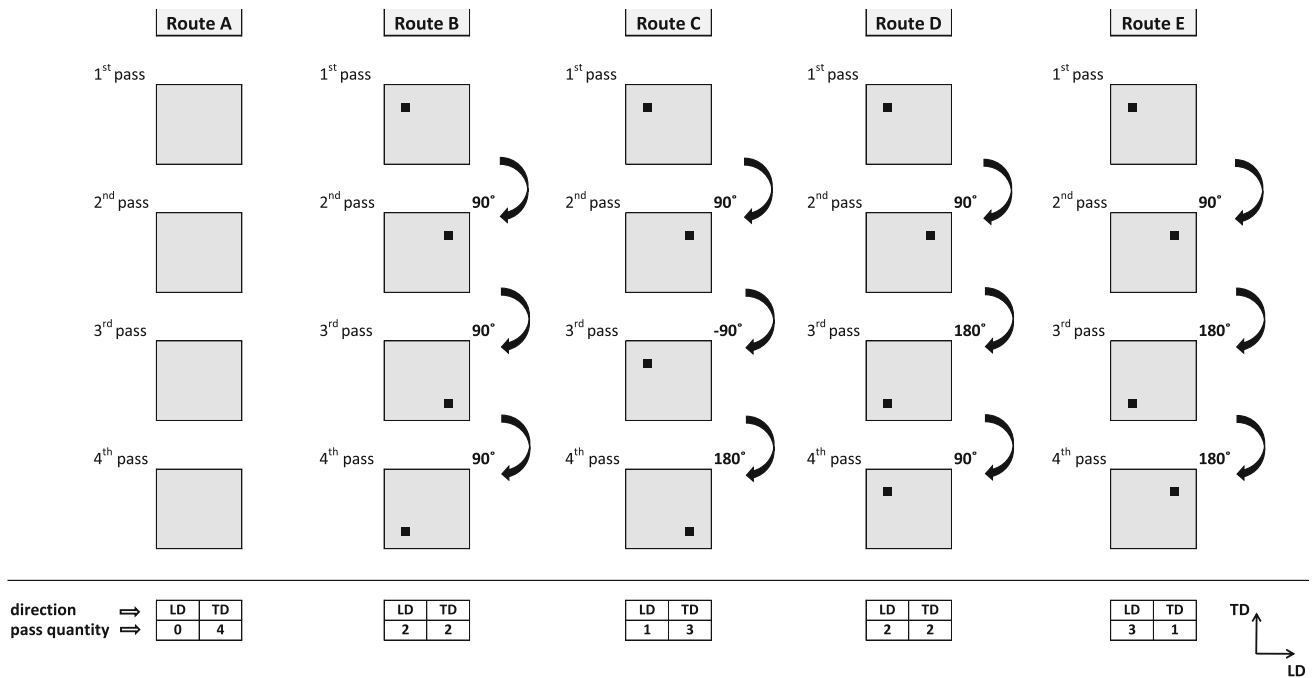


**Fig. 2** Processing schedules for various CGP routes up to 4 passes, where LD and TD stand for the longitudinal and transverse directions, respectively. Each pass constitutes of a set of corrugation and flattening operations

direction (LD) on the central line after each pass to exhibit the homogeneity of the deformation process. Monotonic tensile experiments were performed along the LD and the TD using dog-bone shaped samples having a gage length of 16 mm. Before testing, sample surfaces were ground and polished to eliminate surface irregularities. Tensile loading was carried out with a strain rate of  $0.001 \text{ s}^{-1}$  at ambient temperature. Multiple measurements were conducted for hardness (5 times) and tensile (3 times) tests, and the pertinent variation was exhibited in the results. For microstructural examinations, samples were ground, polished, and etched, using an oxalic acid solution containing 10 g oxalic acid in 100 ml distilled water. Electrolytic etching was conducted at 6 V for 120 s.

### 3 Deformation Modeling

To verify the level of SPD strain imparted via the die used herein, pressing force and accumulated strain during a CGP pass were analyzed using a commercial finite element software with rectangular elements. Since both 3-D and plane strain cases present very similar results, the latter was implemented due to its computational efficiency [20]. Forming dies were assumed to be rigid with a friction coefficient of 0.1. According to the force-upper die stroke

curve (Fig. 3a), the maximum force required for completing a single pass reaches 800 kN. This value is inline with analytical calculations based on bending analysis [21, 22]:

$$F_{\max} = nk \frac{\sigma_u L h^2}{t} \tag{1}$$

where  $n$  is the total number of groove edges,  $t$  is the groove width,  $k$  is determined for AISI 304 based on the die geometry used in this work. Moreover,  $\sigma_u$  is the ultimate tensile strength as determined experimentally,  $L$  and  $h$  are the width and thickness of the workpiece, respectively.

The effective strain per pressing is shown in Fig. 3b. Accordingly, the sheared regions accumulate a strain of  $\sim 0.21$ , resulting in a strain of  $\sim 0.42$  per pass. The following effective strain formulation yields a similar result [22]:

$$\epsilon_{\text{eff}} = \frac{\tan \theta}{\sqrt{3}} \tag{2}$$

where  $\theta$  is the inclination angle. The inclination angle is determined based on measurements on the as-processed samples. For any given route, four CGP passes are applied for accumulating an effective strain of 1.68, representing the level of SPD imposed. This value considers that the applied strain is the same for each pressing and flattening step of a single pass and resembles previous reports [22].

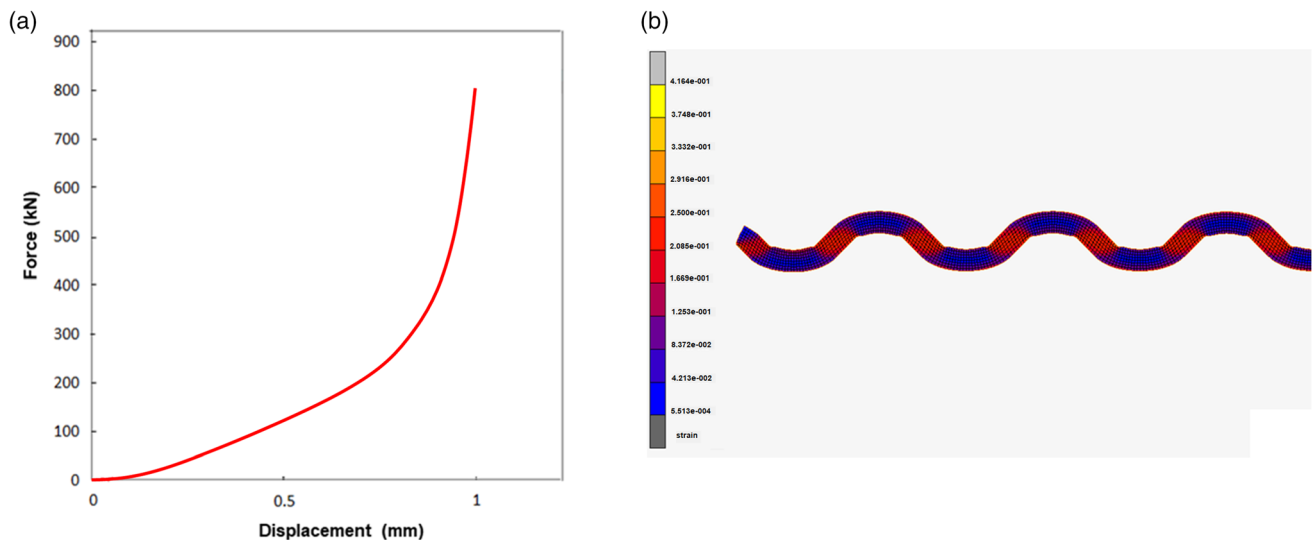


**Fig. 3** **a** Force–displacement curve for a single CGP pass, and **b** corresponding strain distribution in the processed sheet

## 4 Results and Discussion

### 4.1 Microstructural Development

Optical microscopy was utilized in order to analyze the microstructural development of the samples after processing. The average grain size was calculated by using the linear intercept method including 10 vertical and 10 horizontal lines. Microstructure of the as-received material displays annealing twins, with an average grain size (AGS) of 40 microns. Figure 4 demonstrates the microstructural development after CGP. Grain refinement down to an average of 30 microns is observed after a single pass. With respect to the level of refinement, considerable difference has not been recorded among the processing routes after 4 passes leading to an AGS in the range of 20 microns as listed in Table 1. This also indicates that strain path is not influential in dictating the grain size after processing. It is also important to note that activation of mechanical twinning is apparent after SPD.

Typically, the rate of grain refinement slows down with the increase in imposed strain during SPD [23–26]. However, effectiveness of CGP in grain refinement is even lower as compared to other SPD techniques, since it imposes a simple deformation field where slip during groove pressing is cancelled out by reverse slip during flattening [27].

### 4.2 Evaluation of Hardness and Mechanical Response

Effect of processing route on the mechanical properties was probed via hardness and tensile straining experiments. Specifically, hardness measurements reveal the property

variation along the central line of the samples. Moreover, for a quantitative expression of the variation along the LD on the deformed surface perpendicular to ND, inhomogeneity factors (IF) were calculated according to the following expression for each route with increased number of passes [28, 29]:

$$IF = \frac{\sqrt{\left(\sum_{i=1}^n (H_i - \bar{H})^2\right) / (n - 1)}}{\bar{H}} \times 10 \quad (3)$$

where  $H_i$  is the magnitude of each hardness measurement,  $\bar{H}$  is the average hardness, and  $n$  is the total number of measurements.

The highest change in hardness is achieved during the first pass with a 60% increase over the as-received condition. Regardless of the route, the average hardness improvement is over two-folds after the fourth pass (Fig. 5a–e). Inhomogeneity factors for the first passes are approximately the same as seen in Fig. 5f, which is expected since these passes are identical for all routes. With the second pass, IF values decrease and a similar result is anticipated for all the routes except route A in which the sample is not rotated between passes. With increased number of passes, there is some variation in IF values, though route E exhibits the highest uniformity. Considering the small inhomogeneity variation between routes B and D having different pass orders, it can be interpreted that pass order has almost no effect on homogeneity along a specific direction. The greatest difference of uniformity is between routes C and E as expected. First two passes are the same for these routes; but regarding the groove edge orientation, the last two passes of route C are along TD while they are in LD for route E. This induces a higher non-uniformity along LD for route C and a more



**Fig. 4** Microstructure of the CGP processed materials, where few instances of annealing and mechanical twins are indicated by solid and dashed arrows, respectively: **a** after 1 pass; **b** after 4 passes of route A; **c** after 4 passes of route B; **d** after 4 passes of route C; **e** after 4 passes of route D; **f** after 4 passes of route E

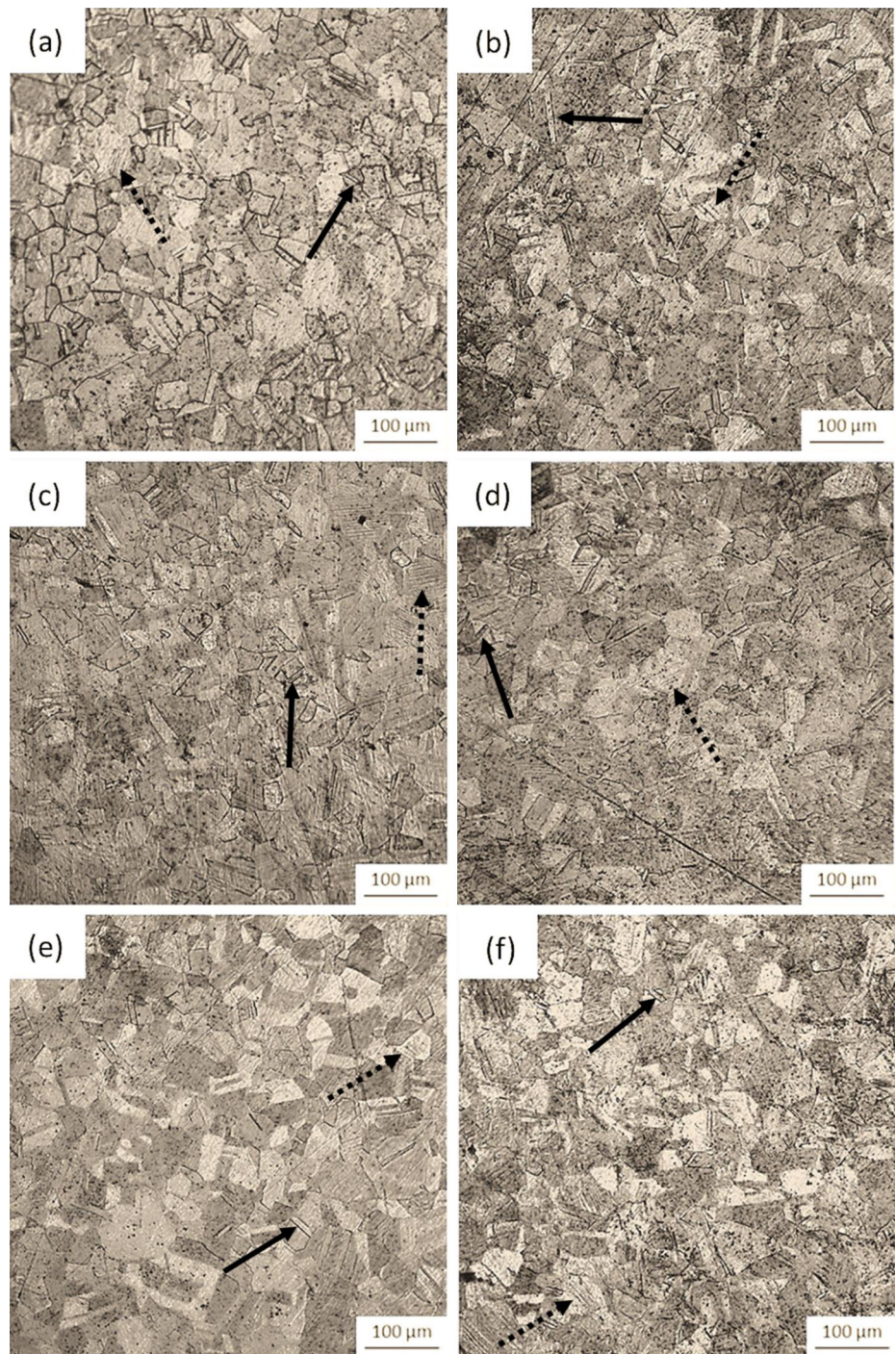


**Table 1** Average grain size values obtained after various processing routes

Condition	As-Received	1 pass	4 passes Route A	4 passes Route B	4 passes Route C	4 passes Route D	4 passes Route E
AGS (μm)	40 ± 1.4	29 ± 1.1	22 ± 0.7	19 ± 0.2	20 ± 0.4	21 ± 0.5	20 ± 0.8

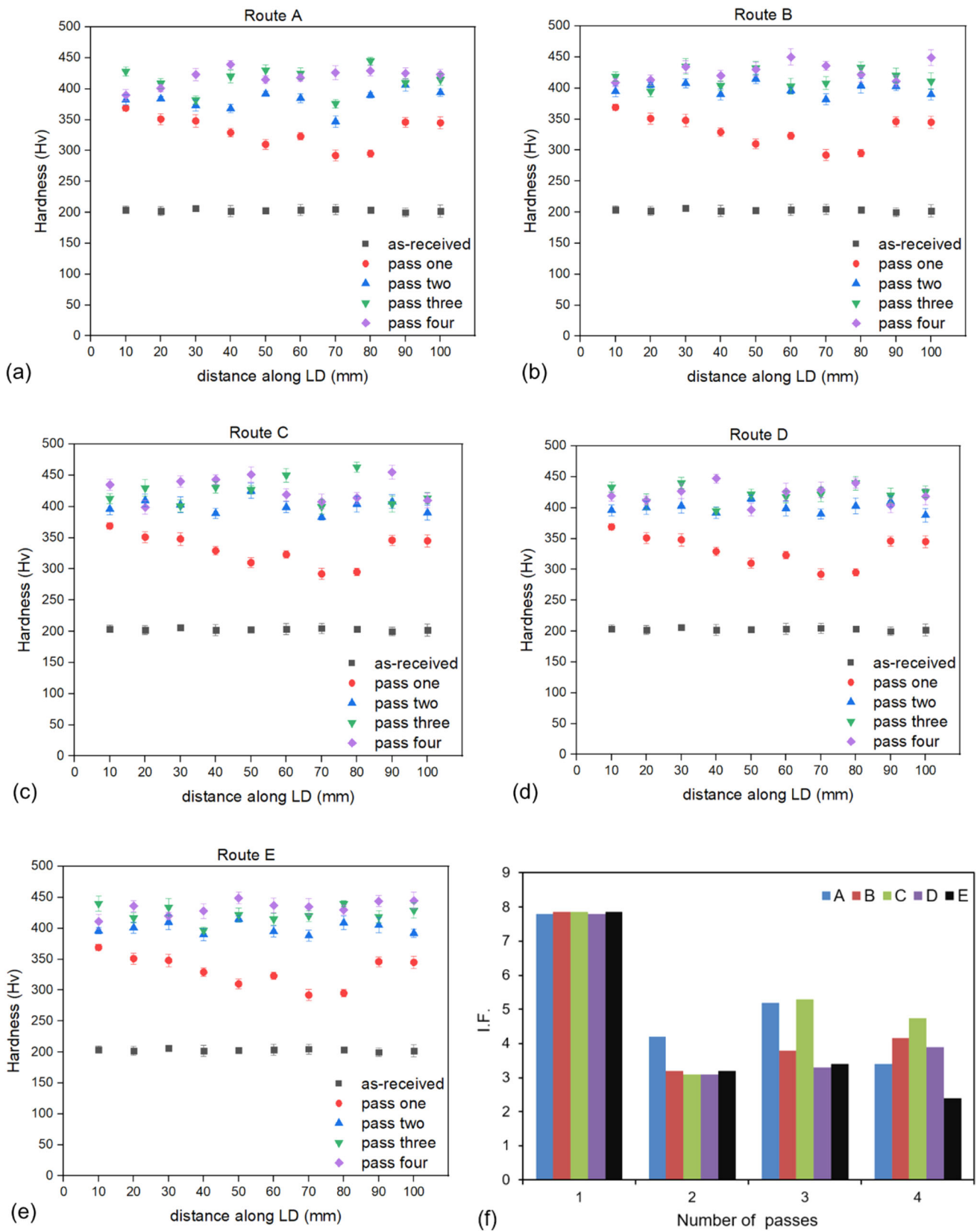


**Fig. 5** a–e Hardness profiles of the CGPed samples for all the routes along the longitudinal distances, f Inhomogeneity factors for all the routes versus pass numbers



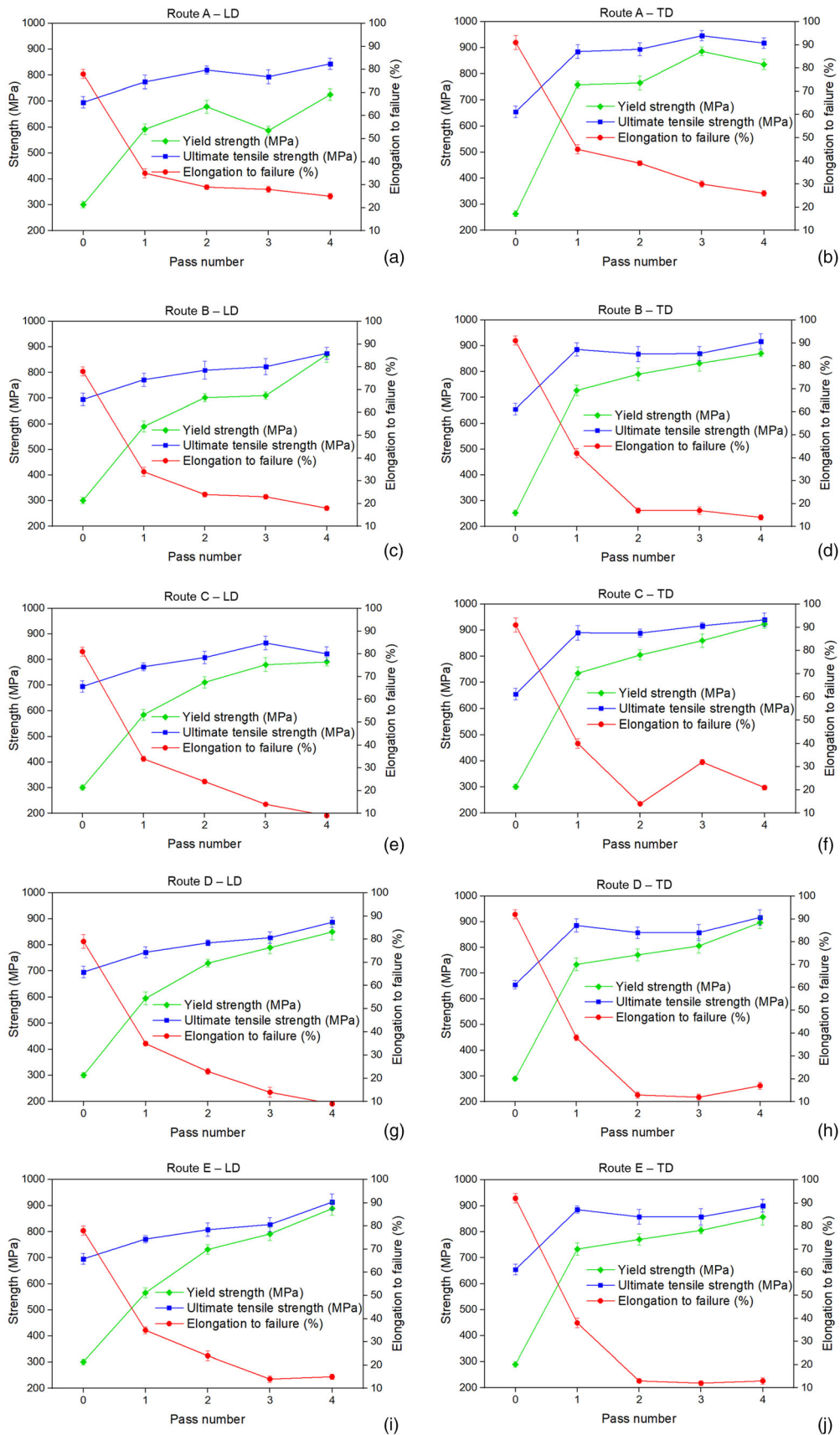


**Fig. 6** Mechanical behavior of processed samples as reflected by the trends in YS, UTS and ductility levels along **a** longitudinal direction and **b** transverse direction

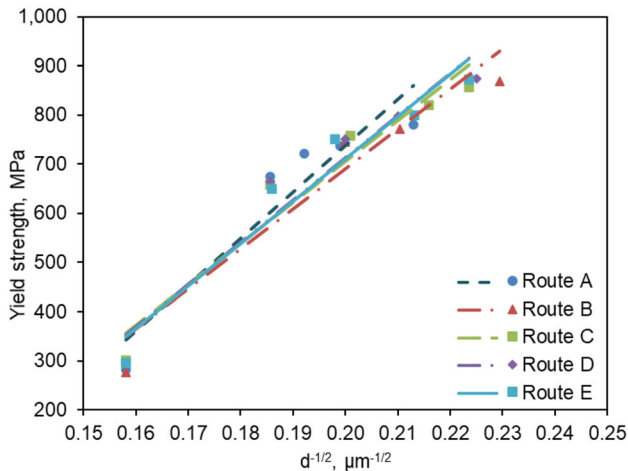


**Fig. 7** Hall–Petch relationship for all the CGP routes demonstrated in this study

uniform deformation for route E [21, 27]. In addition, unlike others, route A has bending deformation applied on a specific region for all the passes along LD and thus should have the greatest inhomogeneity. However, alternating deformation field, in which dislocation generation rate changes over multiple pressing cycles, hinders this drawback [27].

Deformation under tension exhibits that strength improvement after CGP is prevalent for all routes (Fig. 6). Yield strength values increase more than two times for almost all passes. Among the routes examined, strength increases with higher number of passes. The highest strength-ductility combination is achieved for route A samples when tested along TD after three passes. It is also imperative to mention that the strain hardening rate differs with both the pass number and the specific CGP route followed. It is typical that the strain hardening rate during post-SPD deformation decreases with imposed strain during SPD [30], and this is common for all routes with varying magnitude. The ability for strain hardening is preserved at a higher extent for route A samples, especially when tested along TD, explaining their higher levels of elongation to failure.

As a side note, route A yields the highest ductility in both directions after the fourth pass. The ductility values decrease from around 90% to 25% for route A while they range between 10 and 20% for the other routes. Three passes of route A can be considered as a viable processing scheme providing decent strength improvement along with

over 30% failure strain when tested along TD. It should be also underlined that the ductility levels are consistently higher along TD after the first pass, regardless of the strain path. This shows variation depending on the CGP route for the successive passes.

The correlation between yield strength and grain size can be verified in this study according to the Hall–Petch relationship [31, 32]. Based on the slopes in Fig. 7, the average Hall–Petch constant ( $k$ ) is noticeably higher than those previously reported [32, 33]. The dislocation density generated during SPD along with the existence of mechanical twins are two probable mechanisms contributing to this discrepancy [34, 35]. Mechanical twinning has been reported to be an operative deformation mechanism even at temperatures of  $0.6 T_m$  during SPD of austenitic stainless steels [36]. It should be also noted that the Hall–Petch constants as demonstrated by the slope values do not differ considerably for various CGP routes. This indicates that the grain boundary characters do not differ much with respect to the strain path followed.

Grain refinement and strain hardening cause the majority of strengthening during the initial passes compared to the subsequent passes. In fact, strength levels could even degrade with sequential CGP processing due to the mechanisms of micro-cracking and flow softening which is related to dislocation annihilation at higher levels of deformation via dynamic recovery [26]. This has also been shown during SPD of aluminum [37] and copper [38] where occurrence of strength plateau is associated with saturation of dislocation density for strain energy minimization [39]. In a recent work, comparing of rolled and ECAE/P processed copper indicates that these two distinct strain paths lead to only slight variation in the dislocation density levels at similar accumulated plastic strains [38]. Accordingly, it can be asserted that the defect levels will be similar regardless of the CGP route after 4 passes.

Such a plateau behavior may not be present for the hardness measurements. Indeed, for all routes, average hardness levels escalate after successive passes although the increase between the passes is smaller after the first pass. According to this observation, it can be claimed that micro-cracking is more effective than flow softening in the reduction of strength [21]. Strength does not show a monotonic change with increasing pass number for routes A and C. This points to the more likely occurrence of micro-cracks during processing via these routes.

### 4.3 Evaluation of Strength Anisotropy

Mechanical response of the samples strained along two in-plane perpendicular directions reveal the existence of flow anisotropy with varying degree depending on the route and pass number. Since grain size and morphology do not show



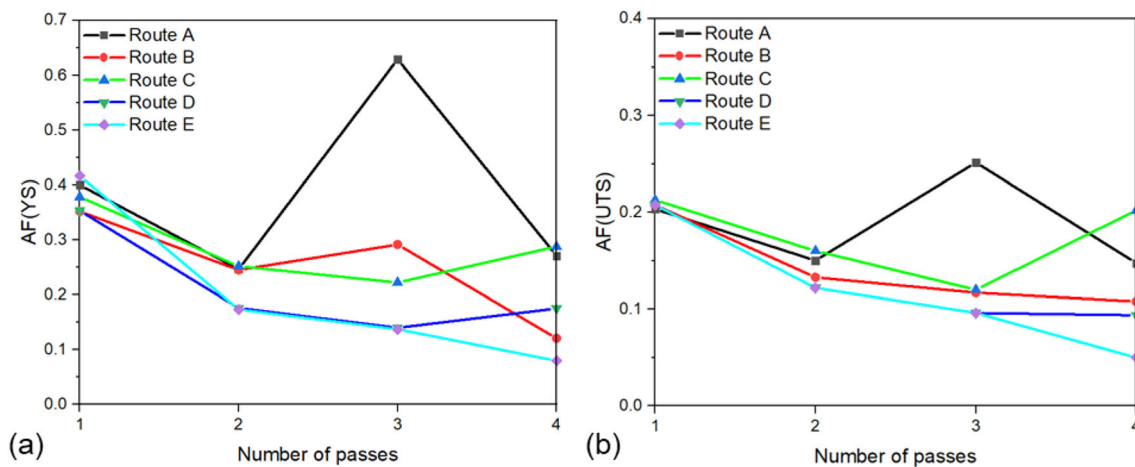


**Fig. 8** Anisotropy factors for all routes examined up to 4 CGP passes for **a** yield strength and **b** ultimate tensile strength

substantial variation with route, strain path-induced texture can be cited as the source of anisotropy [6]. Tensile strength after the last pass along TD is greater than that along LD on all routes except E. For this route, there are three passes for which the groove edges are parallel to LD of the sheet. This implies that number of passes along a specific direction plays a role on the directional strength. The highest strength increase is about 32% and occurs along LD for route E as compared to 41% recorded along TD belonging to route C. This result can be reasoned considering that route C has three passes in which the groove edges are parallel to TD, whereas for route E, the same holds true as parallel to LD.

Examining Fig. 6, it can be disclosed that strength anisotropy levels of routes A and C are relatively higher as compared to the other routes. This is also clear by comparing the anisotropy factors (AF) for each route (Fig. 8). AF is defined for both the yield strength (YS) and the ultimate tensile strength (UTS) as  $AF_{YS} = |YS_{TD} - YS_{LD}| / YS_{LD}$  and  $AF_{UTS} = |UTS_{TD} - UTS_{LD}| / UTS_{LD}$ , respectively. AF values following CGP are calculated by considering the initial anisotropy present in the as-received material. Since the as-received response presents slight strength differential along LD and TD, processing-induced anisotropy is revealed by determining the net AF values. Regardless of the route,  $AF_{YS}$  and  $AF_{UTS}$  follow a similar trend, where the former typically presents higher values. This implies that the degree of anisotropy reduces for UTS and is more severe for YS levels. While route A presents the highest anisotropy in yield strengths after the third pass, that of route C peaks after the last CGP pass.

Rotation between the passes reduces anisotropy because of more uniform distribution of the stretching and bending regions, where SPD takes place and the highest propensity for micro-cracking is expected [25]. Thus, route B is promising in terms of isotropy due to successive rotations

between passes. Similar mechanical responses of routes B and D indicate that pass order has a minor effect on anisotropy. In comparison, routes A and C present a higher degree of anisotropy in relation with their comparably higher number of passes for which the groove edges are parallel to TD of the sheet. Especially for route A, the strain path does not involve any in-plane rotations of the sheet. Therefore, it can be deduced that processing routes containing a sequence of passes with varying directions can be followed to provide isotropic properties. Moreover, the two vital sources of anisotropy are crystallographic texture and morphological texture [40–42]. As the CGP-induced microstructural evolutions exhibit equiaxed morphologies regardless of the strain path, any observed anisotropy shall be linked to crystallographic texture evolution during processing. Thus, apparent LD-TD strength anisotropy with varying degrees shall be attributed to crystallographic texture by effectively dictating the activation of various deformation mechanisms.

## 5 Conclusions

AISI 304 sheets were processed following newly introduced constrained groove pressing routes with varying strain paths. Notable findings of this study are as follows:

1. Microstructural evolution during CGP led to similar size and morphology irrespective of the route followed. Grain refinement resulted in an average grain size level within the range of 20–25 microns.
2. For the first pass, hardness values of the samples increased up to 60%. The highest average value of 432 Hv was achieved after four passes of route E processing. Depending on the route, the increase in yield

strength was more than twice, whereas over 40% increase in tensile strength was apparent.

3. For all routes, similar microstructural evolutions could be traced in terms of grain size and morphology. For microstructural uniformity, route E should be preferred. Considering the negligible difference between routes B and D, it could also be concluded that pass order had no net effect on homogeneity.
4. Route A provided samples with a decent combination of strength and ductility. Anisotropy levels of route A and C were observed to be the highest, whereas routes B and D had desirable isotropy among the routes due to even number of passes applied in a sequence along both directions.

**Acknowledgments** Support from Ozyegin University Research Fund is acknowledged.

## References

- [1] Shin D H, Park J J, Kim Y S, and Park K T, *Mater Sci Eng A* **328** (2002) 98.
- [2] Kumar S S S, and Raghu T, *J Mater Process Technol* **213** (2013) 214.
- [3] Hosseinzadeh A, and Yapici G G, *J Eng Mater Technol, Trans ASME* **143** (2021) 011005. <https://doi.org/10.1115/1.4047966>
- [4] Hosseinzadeh A, and Yapici G G, *Mater Sci Eng A* **731** (2018) 487.
- [5] Sajadifar S V, and Yapici G G, *J Mater Eng Perform* **23** (2014) 1834.
- [6] Yapici G G, Karaman I, and Maier H J, *Mater Sci Eng A* **434** (2006) 294.
- [7] Zhilyaev A P, Lee S, Nurislamova G V, Valiev R Z, and Langdon T G, *Scr Mater* **44** (2001) 2753.
- [8] Zhilyaev A P, and Langdon T G, *Prog Mater Sci* **53** (2008) 893.
- [9] Saito Y, Utsunomiya H, Tsuji N, and Sakai T, *Acta Mater* **47** (1999) 579.
- [10] Jawad D H, Hosseinzadeh A, and Yapici G G, *Mater Res Express* **6** (2019) 096581. <https://doi.org/10.1088/2053-1591/ab2d93>
- [11] Moradpour M, Khodabakhshi F, and Eskandari H, *Mater Sci Technol* **34** (2018) 1003.
- [12] Khodabakhshi F, Abbaszadeh M, Eskandari H, and Mohebpour S R, *J Manuf Process* **15** (2013) 533.
- [13] Krishnaiah A, Chakkingal U, and Venugopal P, *Mater Sci Eng A* **410–411** (2005) 337.
- [14] Nobakht S, and Kazeminezhad M, *Int J Miner Metall Mater* **24** (2017) 1158.
- [15] Zimina M, Bohlen J, Letzig D, Kurz G, Cieslar M, and Zrnik J, *Mater Sci Eng* **63** (2014) 012078.
- [16] Hajizadeh K, Ejtemaei S, and Eghbali B, *Appl Phys A* **123** (2017) 504.
- [17] Soleimani F, and Kazeminezhad M, *Steel Res Int* **89** (2018) 1700548.
- [18] Singh R, Singh D, Sachan D, Yadav S D, and Kumar A, *J Mater Eng Perform* **30** (2021) 290.
- [19] Wang Z, Liang P, Guan Y, Liu Y, and Jiang L, *Indian J Eng Mater Sci* **21** (2013) 121.
- [20] Sajadi A, Ebrahimi M, and Djavanroodi F, *Mater Sci Eng A* **552** (2012) 97.
- [21] Peng K, Su L, Shaw L L, and Qian K W, *Scr Mater* **56** (2007) 987.
- [22] Wang Z S, Guan Y J, Wang G C, and Zhong C K, *J Mater Process Technol* **215** (2015) 205.
- [23] Huang Y, and Prangnell P B, *Acta Mater* **56** (2008) 1619.
- [24] Hebesberger T, Stüwe H P, Vorhauer A, Wetscher F, and Pippan R, *Acta Mater* **53** (2005) 393.
- [25] Jazaeri H, and Humphreys F J, *Acta Mater* **52** (2004) 3239.
- [26] Bowen J R, Prangnell P B, and Humphreys F J, *Mater Sci Technol* **16** (2000) 1246.
- [27] Peng K, Zhang Y, Shaw L L, and Qian K W, *Acta Mater* **57** (2009) 5543.
- [28] Borhani M, and Djavanroodi F, *Mater Sci Eng A* **546** (2012) 1.
- [29] Khodabakhshi F, Kazeminezhad M, and Kokabi A H, *Mater Sci Eng A* **527** (2010) 4043.
- [30] Yapici G G, *Mater Lett* **279** (2020) 128443.
- [31] Mintz B, *Met Technol* **11** (1984) 265.
- [32] Bergstrom Y, and Hallen H, *Met Sci* **17** (1983) 341.
- [33] Karavaeva M V, Abramova M M, Enikeev N A, Raab G I, and Valiev R Z, *Metals* **6** (2016) 310.
- [34] Huang C X, Yang G, Gao Y L, Wu S D, and Zhang Z F, *Mater Sci Eng A* **485** (2008) 643.
- [35] Karaman I, Yapici G G, Chumlyakov Y I, and Kireeva I V, *Mater Sci Eng A* **410–411** (2005) 243.
- [36] Yapici G G, Karaman I, and Luo Z P, *Acta Mater* **54** (2006) 3755.
- [37] Gubicza J, Chinh N Q, Langdon T G, and Ungar T, *Microstructure and Strength of Metals Processed by Severe Plastic Deformation, Ultrafine Grained Materials IV*, TMS **4** (2006) 231.
- [38] Sousa T G, Sordi V L, and Brandao L P, *Mater Res* **21** (2018) 1.
- [39] Hughes D A, and Hansen N, *Acta Mater* **48** (2000) 2985.
- [40] Yapici G G, Tome C N, Bayerlein I J, Karaman I, Vogel S C, and Liu C, *Acta Mater* **57** (2009) 4855.
- [41] Hansen B L, Carpenter J S, Sintay S D, and Gray G T, *Int J Plast* **49** (2013) 71.
- [42] Yapici G G, Bayerlein I J, Karaman I, and Tome C N, *Acta Mater* **55** (2007) 4603.

**Publisher's Note** Springer Nature remains neutral with regard to jurisdictional claims in published maps and institutional affiliations.